Enzyme-powered porous micromotors built from a hierarchical micro- and mesoporous UiO-type metal-organic framework

Yunhui Yang,[#] Xavier Arqué,[#] Tania Patiño,* Vincent Guillerm, Pascal-Raphael Blersch, Javier Pérez-Carvajal, Inhar Imaz,* Daniel Maspoch,* Samuel Sánchez*

ABSTRACT: Enzyme-powered porous micro- and nanomotors combine self-propelled motion with tailored functionalities like adsorption and release, making them very attractive for myriad applications. Here, we report the design, synthesis and functional testing of enzyme-powered porous micromotors built from a metal-organic framework (MOF). We began by subjecting a pre-synthesized microporous UiO-type MOF to ozonolysis, to confer it with mesopores sufficiently large to adsorb and host the enzyme catalase (size: 6-10 nm). We then encapsulated catalase inside the newly-formed mesopores, observing that they are hosted in those mesopores located at the subsurface of the MOF crystals. In the presence of H_2O_2 fuel, our MOF motors (or *MOFtors*) exhibit jet-like propulsion enabled by enzymatic generation of oxygen bubbles. Moreover, thanks to their hierarchical pore system, the MOFtors retain sufficient free space for adsorption of additional targeted species, which we validated by testing a MOFtor for removal of the pollutant Rhodamine B during self-propulsion in water. Our findings will encourage future designs of porous MOF-based micro- and nanomotors for delivery, sorption and catalytic applications.

The field of bio-inspired micro- and nanomotors has evolved extensively so many synthetic structures have been reported over the past decade.[1] From the various ways these tiny motors can be powered, self-propulsion via chemical reactions is one of the most widely used being natural catalysts, such as enzymes, a promising alternative to achieve efficient and biocompatible systems. Several milestones towards real-world applications of such motors have been achieved, primarily in the fields of biomedicine[2-7] and environmental applications.[8-11] In those applications, porosity of the motor chassis is crucial as it enables adsorption, transport and/or release of cargo (*e.g.* drugs or pollutants),[8,12,13] being its performance dictated mainly by its sorption-capacity and its cargo transport-versatility.[14-17]

Among the alternatives available for developing enzyme-powered porous motors, metal-organic frameworks (MOFs) are an attractive choice. MOFs exhibit very high surface areas, tunable pore sizes and shapes, and adjustable pore-surface functionality, suggesting their potential for myriad applications, including gas-storage, separation, catalysis, contaminant removal, and drug delivery.[18,19] In fact, researchers have used MOFs to build stable and adaptable chassis for micro- and nanomotors,[20,21] in which motion is based on Marangoni effects,[22-25] magnetically-driven corkscrew locomotion[26,27] or bubble propulsion[28-34]. For the latter, studies are si far mostly limited to metallic catalytic materials (*e.g.* Ag,[28] Pt,[29,30] Co[31,32] and Mn).[33,34] In parallel, researchers have demonstrated that biomolecules — particularly, enzymes — can be encapsulated within MOFs for protection and to confer the MOFs with new functionalities, mainly in catalysis. For instance, Falcaro, Doonan and co-workers explored biomimetic mineralization and controlled co-precipitation to encapsulate several enzymes in ZIF-8.[35] Another challenging approach has required custom-made linkers to assemble MOFs with pores large enough (mesopores) to adsorb and host enzymes. For instance, the groups of Farha[36] and Zhou[37] exploited MOFs mesopores to encapsulate various enzymes such as organophosphorus acid anhydrolase, glucose oxidase (size: 5.2-7.7 nm), horseradish peroxidase (size: 4.0 nm to 6.8 nm), cytochrome c (size: 2.6-3.3 nm), microperoxidase-11 (size: 1.1-3.3 nm) and tyrosinase (size: 5.5-5.6 nm). Additionally, Ma *et al.* studied the transport phenomena of microperoxidase-11 entering the interior of Tb-mesoMOF pores (size: 3.9-4.7 nm) from solution.[38] Importantly, for a MOF to be used as the chassis of an enzyme-powered porous motor, it must combine mesopores sufficiently large to host the enzyme used for propulsion, with micropores of an appropriate size to adsorb and release additional guest species.

Herein we report the design of an enzyme-powered, porous, MOF-based micromotor via compartmentalized encapsulation of the enzyme catalase within a hierarchical micro- and mesoporous MOF (Figure 1a). We chose catalase as a model enzyme, as it has been extensively used to induce ballistic propulsion through and bubble propulsion via decomposition of H_2O_2.[39-42] Moreover, we selected an UiO-type Zr-MOF as the chassis because of its well-known
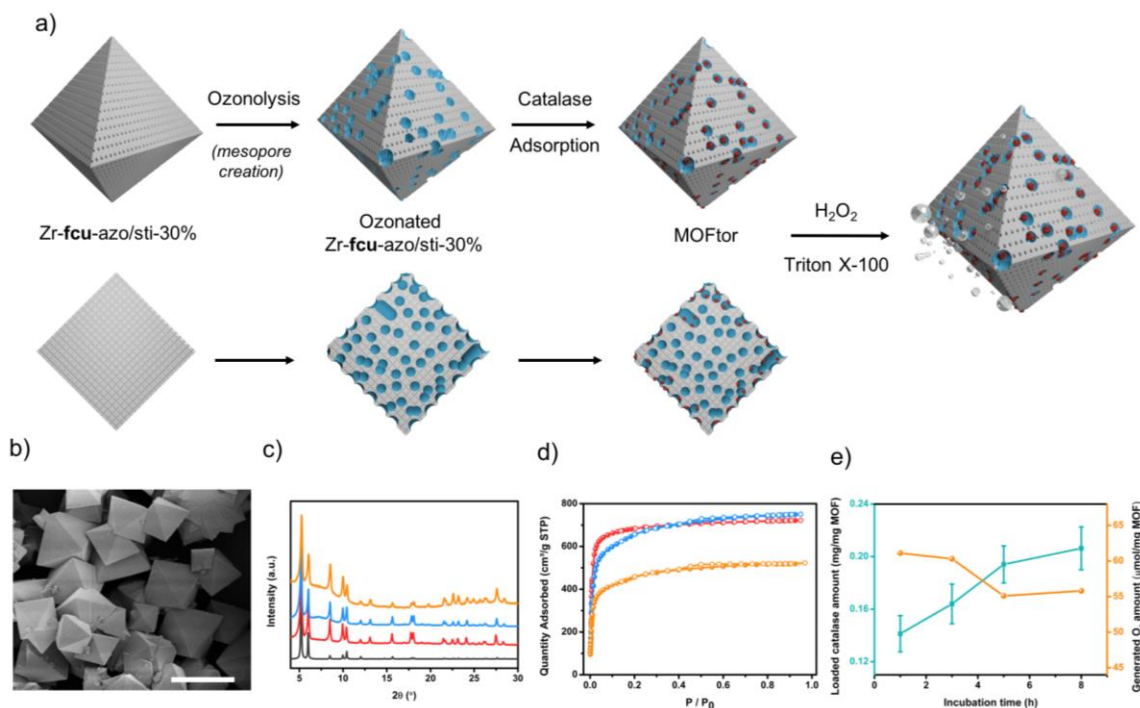
Figure 1. a) Schematic representation of the multi-step process used to synthesize the MOFtors. Bottom images represent cross sections of the octahedral crystals. b) Representative FESEM image of ozonated Zr-**fcu**-azo/sti-30%. Scale bar = 10 μm. c) PXRD diagrams of Zr-**fcu**-azo/sti-30% before (red) and after (blue) ozonolysis, and after catalase encapsulation (orange), in comparison to simulated pattern for Zr-**fcu**-azo (black). d) N_2 isotherms Zr-**fcu**-azo/sti-30% before (red) and after (blue) ozonolysis, and after catalase encapsulation (orange). e) Encapsulation efficiency (blue) and oxygen generated (orange) plotted as a function of time.

water stability;[43] a condition that should fulfil any MOF intended to be used for the fabrication of motors powered by enzymatic reactions. In this design, another essential condition was the use of a UiO-type MOF with mesopores sufficiently large to host catalase (size: 6-10 nm) and micropores that preserve the ability to adsorb and/or release additional guest species. In order to rationally design this MOF, we decided to use an approach that we had developed earlier, whereby we subject pre-synthesized microporous MOFs functionalized with a mixture of linkers that do or do not contain olefins to ozonolysis, which selectively oxidizes the olefins to generate new mesopores.[44,45] To do so, we subjected a pre-synthesized UiO-type MOF to this ozonolysis process, and then exploited the newly-formed mesopores to host the catalase molecules.

We began with the synthesis of a UiO-type Zr-**fcu**-MOF (hereafter called *Zr-**fcu**-azo/sti-30%*), formed by mixing 4,4'-azobenzenedicarboxylic acid (H_2azo) with olefin-containing 4,4'-stilbenedicarboxylic acid (H_2sti) linkers at a molar ratio of 7:3, respectively. Field-Emission Scanning Electron Microscopy (FESEM) revealed the formation of octahedral microcrystals (size: 2-15 μm) characteristic of Zr-**fcu**-MOFs (Figure S3), and powder X-ray diffraction (PXRD; Figure 1c) confirmed the phase purity. Proton nuclear magnetic resonance (^{1}H-NMR) of digested crystals confirmed the formation of Zr-**fcu**-azo/sti-30% in an azo/sti molar ratio of 7:3 (Figure S4). Moreover, N_2 sorption

analysis (77 K) confirmed the microporosity of Zr-**fcu**-azo/sti-30%, with a Brunauer-Emmett-Teller surface area (S_{BET}) of 2830 m²/g (Figures 1d and S5).

Next, we selectively removed the sti linkers and residual Zr(IV) fragments in Zr-**fcu**-azo/sti-30% by our ozonolysis protocol (see above), and washing the ozonated solid with 0.5 M solution of acetic acid in DMF. The washed ozonated Zr-**fcu**-azo/sti-30% particles did not exhibit any marked difference in their octahedral shape and crystallinity compared to the initial non-ozonated samples, as confirmed by FESEM (Figure 1b) and PXRD (Figure 1c). The ozonated Zr-**fcu**-azo/sti-30% was analyzed by ^{1}H-NMR, which revealed the absence of sti linkers, confirming that these linkers had been completely removed from the crystals (Figure S4). The creation of mesopores was confirmed by N_2 sorption tests at 77 K (Figures 1d and S6). The isotherm did not show the type-I shape of the isotherm of the starting MOF: instead, it exhibited a small hysteresis between the adsorption and desorption branch, characteristic of mesoporosity. As expected, ozonolysis treatment reduced the apparent S_{BET} down to 2470 m²/g. However, this decrease was offset by the creation of mesopores, at a proportion of 24%, as derived from the comparison of the total pore volume and Dubinin-Radushkevich equation.[46]

Once we had confirmed the formation of Zr-**fcu**-MOF containing hierarchical porosity, we proceeded to study the adsorption of catalase into the latter. For this, 5 mg of ozonated Zr-**fcu**-azo/sti-30% were incubated in 1 mL of an

aqueous solution of catalase (3 mg/mL) for different periods of time. After each period, the amount of encapsulated catalase was quantified by the standard Bradford protein assay. The amount of catalase confined in the ozonated Zr-**fcu**-azo/sti-30% was gradually increased from 1 h (0.14± 0.01 mg catalase/mg MOF) to 8 h (0.21± 0.01 mg catalase/mg MOF) (Figure 1e). To further demonstrate the encapsulation of catalase into the mesopores, we used confocal laser microscopy to study the spatial distribution of catalase within the Zr-**fcu**-azo/sti-30% crystals. For this, we repeated the encapsulation process over 8 h, using a catalase tagged with the green dye fluorescein isothiocyanate
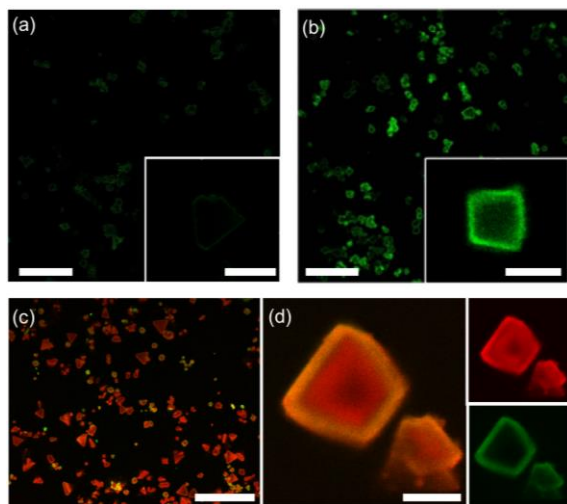

Figure 2. Confocal laser scanning micrographs of a) as-synthesized and b) ozonated Zr-**fcu**-azo/sti-30% crystals after incubation with FITC-tagged catalase (green) for 8 h; and c,d) MOFtors after adsorption of Rhodamine B (red). In d), the left image is the superposition of both right images showing adsorbed Rhodamine B (red, top) and compartmentalized FITC-tagged catalase (green, bottom). Scale bars: 50 μm (a,b,c); 5 μm (inset a, d) and 3 μm (inset b).

(FITC). For comparison, we also repeated this encapsulation process using a non-ozonated Zr-**fcu**-azo/sti-30%, which does not contain mesopores. Confocal micrographs of the ozonated and the non-ozonated Zr-**fcu**-azo/sti-30% demonstrated that catalase is encapsulated only within the crystals of the former, where it is predominantly compartmentalized at the subsurface (Figures 2a,b). We attributed the preferential localization of catalase at the subsurface of each MOF crystal to the initial random distribution of azo- and sti- linkers that, following removal of the latter via ozonolysis, produce crystals in which the meso- and micropores are randomly localized. This makes the external mesoscale cavities more accessible for catalase than the internal ones, as the diffusion of catalase into the internal large cavities is highly restricted by the probability of encountering pores smaller than the size of catalase.

We next studied the self-propulsion of Zr-**fcu**-azo/sti-30% crystals into which we had incorporated catalase (hereafter called *MOFtors*) for 1, 3, 5 or 8 h. For these ex-

periments, we considered earlier reports that bubble-propulsion is improved by the addition of surfactants to the media;[47-51] thus, we recorded the MOFtor crystals in an aqueous solution containing 0.5% H_2O_2 and Triton X-100 at a 0.25% (v/v) concentration. Remarkably, all four samples showed bubble generation and motion capability (Figure 3a), propelling themselves by a thrust of oxygen bubbles released asymmetrically from a point of nucleation (Video S1). Researchers have reported that any cavity in a micromotor structure -in this case in the MOF crystal-, due to porosity, surface-defects or crystal-aggregation, can enable accumulation of oxygen bubbles for jet-like propulsion.[52,53] Thus, our results confirmed development of enzyme-powered MOF particles in which catalase is hosted in the mesopores at the subsurface of each crystal.

Among the MOFtors generated at different incubation times, the one corresponding to 1 h incubation reached the highest maximum speed (2.79 ± 0.55 body-lengths/s). Interestingly, incubation time was indirectly proportional to speed (Figure 3a). To explore this trend, we quantified the enzymatic activity (O_2 production) of the catalase confined inside the MOFtors, using the displacement method. For all samples, the amount of generated O_2 increased during the first 2 min, and then gradually plateaued at a saturation value (Figure S10). The MOFtor from 1 h of incubation generated the greatest amount of O_2 (61.1 μmol/mg MOFtor) and highest speed of O_2-generation ([49 μmol O_2/s]/mg MOFtor) (Figure 1e). These results are consistent with those of the aforementioned motion experiments. We have tentatively attributed this slight decrease in activity and motion to either a certain degree of inactivation of catalase inside the MOF crystals, or to the fact that the catalase molecules diffuse into the interior of MOF crystals more at longer incubation times, thereby complicating both arrival of the H_2O_2 molecules to the enzymes as well as release of the O_2 bubbles produced by the enzymatic reaction.

Once we had confirmed the optimum incubation time of 1 h, we further investigated the motion capabilities of the corresponding MOFtor. Initially, we studied the influence of the surfactant, by reproducing the recording of MOFtors in an aqueous solution containing 0.5% H_2O_2 in the presence and absence of Triton X-100 (Figure 3b,c). Figure 3c shows different snapshots from the video recordings with
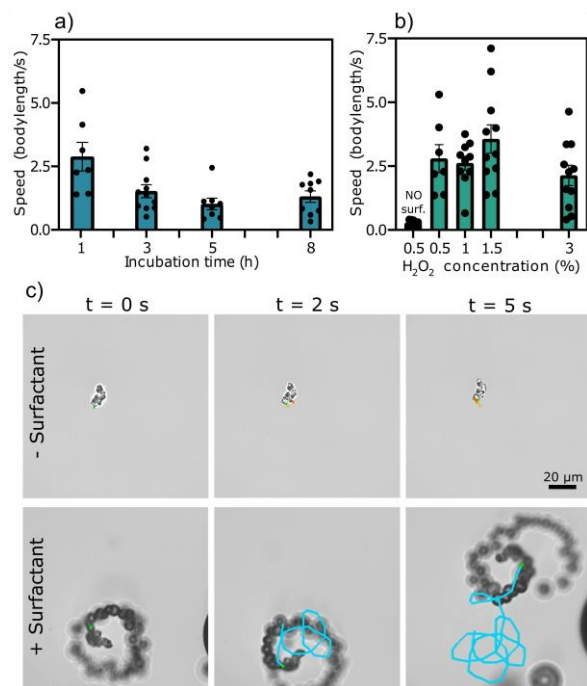

Figure 3. Motion dynamics of enzymatic MOFtors. a) Speed of the MOFtors obtained at different incubation times (1 h, 3 h, 5 h and 8 h). b) Speed of the MOFtors at different H_2O_2 concentrations (0.5% with and without surfactant, and 1.0%, 1.5% and 3.0%). c) Snapshots of the trajectories of the MOFtors at different times in the presence (bottom) or absence (top) of surfactant (0.25% Triton X-100).

their corresponding trajectories where, as previously described, MOFtors in a Triton X-100 dilution displayed high bubble-production, leading to propulsion (Video S2). However, in the absence of surfactant (Figure 3c), we did not observe any bubbles or self-propulsion. We reasoned that the surfactant in the medium reduced the surface tension of the liquid, which in turn promoted formation of and stabilized the bubbles.[39] Similar effects were observed for hollow capsules containing Pt, where enhanced diffusion was reported without surfactant and very aggressive bubble propulsion was observed when surfactant was added to the solution.[54] We also assessed the self-propulsion of the MOFtor as a function of fuel (H_2O_2) concentration (Figure 3b). We observed self-propulsion at low surfactant and fuel concentrations[55] compared to those in other studies, in which 3% to 5% H_2O_2 was considered to be a low concentration.[52] Thus, when we increased the H_2O_2 concentration to 1.5%, the self-propulsion increased, reaching a maximum speed of 3.56 ± 0.56 body-lengths/s (Video S3). Regardless, minimizing the concentration of

H_2O_2 required for propulsion is important for biological and environmental applications, given the toxicity of this fuel.

Given that our MOFtor combines both meso- and micropores, and that the catalase enzymes are encapsulated mainly in the mesopores located at the crystal sub-surface, we envisioned using the remaining empty meso- and micropores to adsorb other guest molecules. To this end, N_2-sorption measurements first confirmed that MOFtors has accessible porosity, with an S_{BET} of 1715 m²/g, and that their mesopore proportion is 20%.

Next, reflecting on potential uses for these remaining pores, we considered environmental applications in which we could exploit the available pores to store a pollutant, while using the more-external mesopores for enzymatic bubble propulsion. Thus, we studied the capacity of our MOFtors to capture Rhodamine B, a common water pollutant from the textile, plastic and dye industries, during self-propulsion in water. To this end, catalase-powered MOFtors (5 mg) were dispersed in an aqueous solution (1 mL) of 0.5 mg/mL Rhodamine B and 1.5% H_2O_2 at room temperature. After 30 min of incubation, the Rhodamine B content adsorbed by the MOFtors was determined by UV-Vis spectrometry. The observed extraction was highly efficient: the particles had captured 99.860 ± 0.003 % of the Rhodamine B from the solution. Adsorption of Rhodamine B was also confirmed by confocal microscopy. Indeed, Figures 2c,d show that, while catalase remains localized at the sub-surface of the crystals, Rhodamine B molecules are captured and adsorbed throughout the entire crystal.

In conclusion, we have reported the design, synthesis and functional testing of enzyme-powered MOF-based porous motors. The multi-step synthesis involves generating new mesopores in a pre-synthesized microporous UiO-66-type MOF, via ozonolysis. The resultant MOF contains meso- and micropores. We exploited the newly-generated mesopores to adsorb and host molecules of the enzyme catalase, which were compartmentalized at the subsurface of each MOF crystal. This localized encapsulation of catalase enabled jet-like bubble propulsion of the MOF crystals using H_2O_2 as fuel, even at very low concentrations. Moreover, the remaining unoccupied micro- and mesopores in these MOFtors can be used for adsorbing additional species, as we demonstrated with capture of the pollutant Rhodamine B in water. Our work demonstrates the versatility of MOFs as the structural basis of enzyme-powered porous motors for delivery, sorption and catalytic applications.

ASSOCIATED CONTENT

The Supporting Information is available free of charge via the Internet at http://pubs.acs.org.

Chemicals, instrumentation, synthetic procedures, FESEM, XRPD, porosity data, and videos showing MOFtor movement.

AUTHOR INFORMATION

Corresponding Authors

Tania Patiño - *Institute for Bioengineering of Catalonia (IBEC), The Barcelona Institute of Science and Technology (BIST), Baldiri i Reixac 10-12, 08028 Barcelona, Spain; Chemistry Department, University of Rome, Tor Vergata, Via della Ricerca Scientifica, 00133 Rome, Italy;* E-mail: *tpatino@ibecbarcelona.eu*

Inhar Imaz - *Catalan Institute of Nanoscience and Nanotechnology (ICN2), CSIC and Barcelona Institute of Science and Technology, Campus UAB, Bellaterra, 08193 Barcelona, Spain;* E-mail: inhar.imaz@icn2.cat

Daniel Maspoch - *Catalan Institute of Nanoscience and Nanotechnology (ICN2), CSIC and Barcelona Institute of Science and Technology, Campus UAB, Bellaterra, 08193 Barcelona, Spain; ICREA, Pg. Lluís Companys 23, Barcelona, 08010, Spain;* E-mail: daniel.maspoch@icn2.cat

Samuel Sánchez - *Institute for Bioengineering of Catalonia (IBEC), The Barcelona Institute of Science and Technology (BIST), Baldiri i Reixac 10-12, 08028 Barcelona, Spain; ICREA, Pg. Lluís Companys 23, Barcelona, 08010, Spain;* E-mail: *ssanchez@ibecbarcelona.eu*

Authors

Yunhui Yang - *Catalan Institute of Nanoscience and Nanotechnology (ICN2), CSIC and Barcelona Institute of Science and Technology, Campus UAB, Bellaterra, 08193 Barcelona, Spain.*

Xavier Arqué - *Institute for Bioengineering of Catalonia (IBEC), The Barcelona Institute of Science and Technology (BIST), Baldiri i Reixac 10-12, 08028 Barcelona, Spain.*

Vincent Guillerm - *Catalan Institute of Nanoscience and Nanotechnology (ICN2), CSIC and Barcelona Institute of Science and Technology, Campus UAB, Bellaterra, 08193 Barcelona, Spain.*

Present address: Functional Materials Design, Discovery and Development Research Group (FMD3), Advanced Membranes and Porous Materials Center (AMPM), Division of Physical Sciences and Engineering (PSE), King Abdullah University of Science and Technology (KAUST), Thuwal 23955-6900, Saudi Arabia.

Pascal Blersch - *Institute for Bioengineering of Catalonia (IBEC), The Barcelona Institute of Science and Technology (BIST), Baldiri i Reixac 10-12, 08028 Barcelona, Spain.*

Javier Pérez-Carvajal - *Catalan Institute of Nanoscience and Nanotechnology (ICN2), CSIC and Barcelona Institute of Science and Technology, Campus UAB, Bellaterra, 08193 Barcelona, Spain.*

Authors Contributions

# Y.Y. and X.A.: These authors contributed equally to this work.

ACKNOWLEDGMENT

REFERENCES

(1)   Sánchez, S.; Soler, L.; Katuri, J. Chemically Powered Micro- and Nanomotors. *Angew. Chemie - Int. Ed.* **2015**, *54* (5), 1414–1444.

(2)   Ou, J.; Liu, K.; Jiang, J.; Wilson, D. A.; Liu, L.; Wang, F.; Wang, S.; Tu, Y.; Peng, F. Micro-/Nanomotors toward Biomedical Applications: The Recent Progress in Biocompatibility. *Small* **2020**, *1906184*, 1–16.

(3)   Wang, S.; Liu, X.; Wang, Y.; Xu, D.; Liang, C.; Guo, J.; Ma, X. Biocompatibility of Artificial Micro/Nanomotors for Use in Biomedicine. *Nanoscale* **2019**, *11* (30), 14099–14112.

(4)   Li, J.; Esteban-Fernández de Ávila, B.; Gao, W.; Zhang, L.; Wang, J. Micro/Nanorobots for Biomedicine: Delivery, Surgery, Sensing, and Detoxification. *Sci. Robot.* **2017**, *2* (4), eaam6431.

(5)   Joseph, A.; Contini, C.; Cecchin, D.; Nyberg, S.; Ruiz-Perez, L.; Gaitzsch, J.; Fullstone, G.; Tian, X.; Azizi, J.; Preston, J.; et al. Chemotactic Synthetic Vesicles: Design and Applications in Blood-Brain Barrier Crossing. *Sci. Adv.* **2017**, *3* (8), e1700362.

(6)   Wang, J.; Toebes, B. J.; Plachokova, A. S.; Liu, Q.; Deng, D.; Jansen, J. A.; Yang, F.; Wilson, D. A. Self-Propelled PLGA Micromotor with Chemotactic Response to Inflammation. *Adv. Healthc. Mater.* **2020**, *1901710*, 1–8.

(7)   Wu, Y.; Lin, X.; Wu, Z.; Möhwald, H.; He, Q. Self-Propelled Polymer Multilayer Janus Capsules for Effective Drug Delivery and Light-Triggered Release. *ACS Appl. Mater. Interfaces* **2014**, *6* (13), 10476–10481.

(8)   Parmar, J.; Vilela, D.; Villa, K.; Wang, J.; Sánchez, S. Micro- and Nanomotors as Active Environmental Microcleaners and Sensors. *J. Am. Chem. Soc.* **2018**, *140* (30), 9317–9331.

(9)   Guix, M.; Orozco, J.; Gracía, M.; Gao, W.; Sattayasamitsathit, S.; Merkoçi, A.; Escarpa, A.; Wang, J. Superhydrophobic Alkanethiol-Coated Microsubmarines for Effective Removal of Oil. *ACS Nano* **2012**, *6* (5), 4445–4451.

(10)   Gao, W.; Wang, J. The Environmental Impact of Micro / Nanomachines : A Review. *ACS Nano* **2014**, *8* (4), 3170–3180.

(11)   Orozco, J.; García-Gradilla, V.; D'Agostino, M.; Gao, W.; Cortés, A.; Wang, J. Artificial Enzyme-Powered Microfish for Water-Quality Testing. *ACS Nano* **2013**, *7* (1), 818–824.

(12)   Medina-Sánchez, M.; Xu, H.; Schmidt, O. G. Micro- and Nano-Motors: The New Generation of Drug Carriers. *Ther. Deliv.* **2018**, *9* (4), 303–316.

(13)   Eskandarloo, H.; Kierulf, A.; Abbaspourrad, A. Nano- and Micromotors for Cleaning Polluted Waters: Focused Review on Pollutant Removal Mechanisms. *Nanoscale* **2017**, *9* (37), 13850–13863.

(14)   Llopis-Lorente, A.; Garciá-Fernández, A.; Murillo-Cremaes,

N.; Hortelaõ, A. C.; Patiño, T.; Villalonga, R.; Sancenón, F.; Martínez-Máñez, R.; Sánchez, S. Enzyme-Powered Gated Mesoporous Silica Nanomotors for on-Command Intracellular Payload Delivery. *ACS Nano* **2019**, *13* (10), 12171–12183.

(15) Hortelão, A. C.; Patiño, T.; Perez-Jiménez, A.; Blanco, À.; Sánchez, S. Enzyme-Powered Nanobots Enhance Anticancer Drug Delivery. *Adv. Funct. Mater.* **2017**, *28* (25), 1–10.

(16) Wu, Y.; Lin, X.; Wu, Z.; Möhwald, H.; He, Q. Self-Propelled Polymer Multilayer Janus Capsules for Effective Drug Delivery and Light-Triggered Release. *ACS Appl. Mater. Interfaces* **2014**, *6* (13), 10476–10481.

(17) Llopis-Lorente, A.; García-Fernández, A.; Lucena-Sánchez, E.; Díez, P.; Sancenón, F.; Villalonga, R.; Wilson, D. A.; Martínez-Máñez, R. Stimulus-Responsive Nanomotors Based on Gated Enzyme-Powered Janus Au-Mesoporous Silica Nanoparticles for Enhanced Cargo Delivery. *Chem. Commun.* **2019**, *55* (87), 13164–13167.

(18) Themed Issue Metal-Organic Frameworks: *Chem. Soc. Rev.* Zhou, H. C., Kitagawa, S., Eds.; **2014**, *43* (5), 5415– 6172.

(19) Themed Issue Porous Framework Chemistry: *Chem. Rev.* Long, J.; Dinca, M., Eds; **2020**, *120* (16), 8037-9014.

(20) Terzopoulou, A.; Nicholas, J. D.; Chen, X.-Z.; Nelson, B. J.; Pané, J.; Puigmartí-Luis, J. Metal-Organic Frameworks in Motion. *Chem. Rev.* **2020**, doi.org/10.1021/acs.chemrev.0c00535.

(21) Khezri, B.; Pumera, M. Metal–Organic Frameworks Based Nano/Micro/Millimeter-Sized Self-Propelled Autonomous Machines. *Adv. Mater.* **2019**, *31* (14), 1–11.

(22) Ikezoe, Y.; Fang, J.; Wasik, T. L.; Shi, M.; Uemura, T.; Kitagawa, S.; Matsui, H. Peptide-Metal Organic Framework Swimmers That Direct the Motion toward Chemical Targets. *Nano Lett.* **2015**, *15* (6), 4019–4023.

(23) Ikezoe, Y.; Washino, G.; Uemura, T.; Kitagawa, S.; Matsui, H. Autonomous Motors of a Metal-Organic Framework Powered by Reorganization of Self-Assembled Peptides at Interfaces. *Nat. Mater.* **2012**, *11* (12), 1081–1085.

(24) Ikezoe, Y.; Fang, J.; Wasik, T. L.; Uemura, T.; Zheng, Y.; Kitagawa, S.; Matsui, H. Peptide Assembly-Driven Metal-Organic Framework (MOF) Motors for Micro Electric Generators. *Adv. Mater.* **2015**, *27* (2), 288–291.

(25) Park, J. H.; Lach, S.; Polev, K.; Granick, S.; Grzybowski, B. A. Metal-Organic Framework "Swimmers" with Energy-Efficient Autonomous Motility. *ACS Nano* **2017**, *11* (11), 10914–10923.

(26) Wang, X.; Chen, X. Z.; Alcântara, C. C. J.; Sevim, S.; Hoop, M.; Terzopoulou, A.; de Marco, C.; Hu, C.; de Mello, A. J.; Falcaro, P.; et al. MOFBOTS: Metal–Organic-Framework-Based Biomedical Microrobots. *Adv. Mater.* **2019**, *31* (27), 2–8.

(27) Terzopoulou, A.; Wang, X.; Chen, X. Z.; Palacios-Corella, M.; Pujante, C.; Herrero-Martín, J.; Qin, X. H.; Sort, J.; J de-Mello, A.; Nelson, B. J.; Puigmartí-Luis, J.; Pané, S. Biodegradable Metal–Organic Framework-Based Microrobots (MOFBOTs). *Adv. Healthc. Mater.* **2020**, 2001031.

(28) Wang, R.; Guo, W.; Li, X.; Liu, Z.; Liu, H.; Ding, S. Highly Efficient MOF-Based Self-Propelled Micromotors for Water Purification. *RSC Adv.* **2017**, *7* (67), 42462–42467.

(29) Ayala, A.; Carbonell, C.; Imaz, I.; Maspoch, D. Introducing Asymmetric Functionality into MOFs: Via the Generation of Metallic Janus MOF Particles. *Chem. Commun.* **2016**, *52* (29), 5096–5099.

(30) Ying, Y.; Pourrahimi, A. M.; Sofer, Z.; Matějková, S.; Pumera, M. Radioactive Uranium Preconcentration via Self-Propelled Autonomous Microrobots Based on Metal-Organic Frameworks. *ACS Nano* **2019**, *13* (10), 11477–11487.

(31) Wang, L.; Zhu, H.; Shi, Y.; Ge, Y.; Feng, X.; Liu, R.; Li, Y.; Ma, Y.; Wang, L. Novel Catalytic Micromotor of Porous Zeolitic Imidazolate Framework-67 for Precise Drug Delivery. *Nanoscale* **2018**, *10* (24), 11384–11391.

(32) Tan, T. T. Y.; Cham, J. T. M.; Reithofer, M. R.; Andy Hor, T. S.; Min Chin, J. Motorized Janus Metal Organic Framework

(33) Li, J.; Yu, X.; Xu, M.; Liu, W.; Sandraz, E.; Lan, H.; Wang, J.; Cohen, S. M. Metal-Organic Frameworks as Micromotors with Tunable Engines and Brakes. *J. Am. Chem. Soc.* **2017**, *139* (2), 611–614.

(34) Liu, J.; Li, J.; Wang, G.; Yang, W.; Yang, J.; Liu, Y. Bioinspired Zeolitic Imidazolate Framework (ZIF-8) Magnetic Micromotors for Highly Efficient Removal of Organic Pollutants from Water. *J. Colloid Interface Sci.* **2019**, *555*, 234–244.

(35) Liang, K.; Coghlan, C. J.; Bell, S. G.; Doonan, C.; Falcaro, P. Enzyme encapsulation in zeolitic imidazolate frameworks: a comparison between controlled co-precipitation and biomimetic mineralisation. *Chem. Commun.* **2016**, *52* (3), 473-476.

(36) Peng, L.; Moon, S-Y; Guelta, M. A.; Lin, L.; Gómez-Gualdrón, D. A., Snurr, R. Q., Harvey, S. P.; Hupp, J. T.; Farha, O. K. Nanosizing a Metal–Organic Framework Enzyme Carrier for Accelerating Nerve Agent Hydrolysis. *ACS Nano* **2016**, *10*, 9174-9182.

(37) Lian, X.; Chen, Y.-P.; Liu, T.-F.; Zhou, H,-C. Coupling two enzymes into a tandem nanoreactor utilizing a hierarchically structured MOF. *Chem. Sci.* **2016**, *7*, 6969-6973

(38) Chen, Y.; Han, S.; Li, X.; Valencia, V.; Zhang, Z.; Ma, S. Why Does Enzyme Not Leach from Metal–Organic Frameworks (MOFs)? Unveiling the Interactions between an Enzyme Molecule and a MOF. *Inorg. Chem.* **2014**, *53* (19), 10006-10008.

(39) Sánchez, S.; Solovev, A. A.; Mei, Y.; Schmidt, O. G. Dynamics of Biocatalytic Microengines Mediated by Variable Friction Control. *Adv. Funct. Mater.* **2010**, *132* (38), 13144–13145.

(40) Sitt, A.; Soukupova, J.; Miller, D.; Verdi, D.; Zboril, R.; Hess, H.; Lahann, J. Microscale Rockets and Picoliter Containers Engineered from Electrospun Polymeric Microtubes. *Small* **2016**, *12* (11), 1432–1439.

(41) Singh, V. V.; Kaufmann, K.; Esteban-Fernández de Ávila, B.; Uygun, M.; Wang, J. Nanomotors Responsive to Nerve-Agent Vapor Plumes. *Chem. Commun.* **2016**, *52* (16), 3360–3363.

(42) Wu, Z.; Lin, X.; Zou, X.; Sun, J.; He, Q. Biodegradable Protein-Based Rockets for Drug Transportation and Light-Triggered Release. *ACS Appl. Mater. Interfaces* **2015**, *7* (1), 250–255.

(43) Cavka, J. H.; Jakobsen, S.; Olsbye, U.; Guillou, N.; Lamberti, C.; Bordiga, S.; Lillerud, K. P. A New Zirconium Inorganic Building Brick Forming Metal Organic Frameworks with Exceptional Stability. *J. Am. Chem. Soc.* **2008**, *130* (42), 13850–13851.

(44) Albalad, J.; Xu, H.; Gándara, F.; Haouas, M.; Martineau-Corcos, C.; Mas-BAllesté, R.; Barnett, S. A.; Juanhuix, J.; Imaz, I.; Maspoch, D. Single-Crystal-to-Single-Crystal Postsynthetic Modification of a Metal–Organic Framework via Ozonolysis. *J. Am. Chem. Soc.* **2018**, *140* (6), 2028–2031.

(45) Guillerm, V.; Xu, H; Albalada, J.; Imaz, I.; Maspoch, D. Postsynthetic Selective Ligand Cleavage by Solid–Gas Phase Ozonolysis Fuses Micropores into Mesopores in Metal–Organic Frameworks. *J. Am. Chem. Soc.* **2018**, *140* (44), 15022–15030.

(46) Dubinin, M. M.; Zaverina, E. D.; Radushkevich, L. V.; Sorbtsiya, I. Struktura Aktivnykh Uglei o.1. Issledovanie Adsorbtsii Organicheskikh Parov. *Zh. Fiz. Khim.* **1947**, *21* (11), 1351– 1362.

(47) Simmchen, J.; Magdanz, V.; Sánchez, S.; Chokmaviroj, S.; Ruiz-Molina, D.; Baeza, A.; Schmidt, O. G. Effect of Surfactants on the Performance of Tubular and Spherical Micromotors - a Comparative Study. *RSC Adv.* **2014**, *4* (39), 20334–20340.

(48) Manesh, K. M.; Cardona, M.; Yuan, R.; Clark, M.; Kagan, D.; Balasubramanian, S.; Wang, J. Template-Assisted Fabrication of Salt-Independent Catalytic Tubular Microengines. *ACS Nano* **2010**, *4* (4), 1799–1804.

(49) Solovev, A. A.; Sánchez, S.; Pumera, M.; Mei, Y. F.; Schmidt,

O. C. Magnetic Control of Tubular Catalytic Microbots for the Transport, Assembly, and Delivery of Micro-Objects. *Adv. Funct. Mater.* **2010**, *20* (15), 2430–2435.

(50) Solovev, A. A.; Sánchez, S.; Mei, Y.; Schmidt, O. G. Tunable Catalytic Tubular Micro-Pumps Operating at Low Concentrations of Hydrogen Peroxide. *Phys. Chem. Chem. Phys.* **2011**, *13* (21), 10131–10135.

(51) Solovev, A. A.; Mei, Y.; Ureña, E. B.; Huang, G.; Schmidt, O. G. Catalytic Microtubular Jet Engines Self-Propelled by Accumulated Gas Bubbles. *Small* **2009**, *5* (14), 1688–1692.

(52) Chi, Q.; Wang, Z.; Tian, F.; You, J.; Xu, S. A Review of Fast Bubble-Driven Micromotors Powered by Biocompatible Fuel: Low-Concentration Fuel, Bioactive Fluid and Enzyme. *Micromachines* **2018**, *9* (10), 537.

(53) Fomin, V. M.; Hippler, M.; Magdanz, V.; Soler, L.; Sánchez, S.; Schmidt, O. G. Propulsion Mechanism of Catalytic Microjet Engines. *IEEE Trans. Robot.* **2014**, *30* (1), 40–48.

(54) Ma, X.; Jang, S.; Popescu, M. N.; Uspal, W. E.; Miguel-López, A.; Hahn, K.; Kim, D. P.; Sánchez, S. Reversed Janus Micro/Nanomotors with Internal Chemical Engine. *ACS Nano* **2016**, *10* (9), 8751–8759.

(55) Solovev, A. A.; Sánchez, S.; Mei, Y.; Schmidt, O. G. Tunable Catalytic Tubular Micro-Pumps Operating at Low Concentrations of Hydrogen Peroxide. *Phys. Chem. Chem. Phys.* **2011**, *13* (21), 10131–10135.

Microporous MOF → (Ozonolysis) → Hierarchical Micro-/Mesoporous MOF → (Catalase Adsorption, H_2O_2, Triton X-100) → Enzyme-powered MOFtor